Inversion of Perceived Direction of Motion Caused by Spatial Undersampling in Two Children with Periventricular Leukomalacia

Maria Concetta Morrone[1,2], Andrea Guzzetta[3], Francesca Tinelli[3,4], Michela Tosetti[3], Michela Del Viva[2,5], Domenico Montanaro[6], David Burr[2,5,7], and Giovanni Cioni[3,4]

Abstract

■ We report here two cases of two young diplegic patients with cystic periventricular leukomalacia who systematically, and with high sensitivity, perceive translational motion of a random-dot display in the opposite direction. The apparent inversion was specific for translation motion: Rotation and expansion motion were perceived correctly, with normal sensitivity. It was also specific for random-dot patterns, not occurring with gratings. For the one patient that we were able to test extensively, contrast sensitivity for static stimuli was normal, but was very low for direction discrimination at high spatial frequencies and all temporal frequencies. His optokinetic nystagmus movements were normal but he was unable to track a single translating target, indicating a perceptual origin of the tracking deficit. The severe deficit for motion perception was also evident in the seminatural situation of a driving simulation video game. The perceptual deficit for trans-

lational motion was reinforced by functional magnetic resonance imaging studies. Translational motion elicited no response in the MT complex, although it did produce a strong response in many visual areas when contrasted with blank stimuli. However, radial and rotational motion produced a normal pattern of activation in a subregion of the MT complex. These data reinforce the existent evidence for independent cortical processing for translational, and circular or radial flow motion, and further suggest that the two systems have different vulnerability and plasticity to prenatal damage. They also highlight the complexity of visual motion perception, and how the delicate balance of neural activity can lead to paradoxical effects such as consistent misperception of the direction of motion. We advance a possible explanation of a reduced spatial sampling of the motion stimuli and report a simple model that simulates well the experimental results. ■

INTRODUCTION

In humans, motion is analyzed at various cortical levels, including the primary and secondary visual cortex (V1/V2). The major area specialized for motion analysis is the human MT complex, the homologue of the monkey middle temporal cortex MT or V5 (Tootell et al., 1995; Zeki et al., 1991; Zeki, 1980). Neural activity in this region (in humans) shows strong motion opponency (Heeger, Boynton, Demb, Seidemann, & Newsome, 1999), increases linearly with motion coherence (Rees, Friston, & Koch, 2000), and has been shown (in monkey and human) to correlate closely with motion perception (Rees et al., 2000; Britten, Newsome, Shadlen, Celebrini, & Movshon, 1996). Other areas include a portion of V3 (Smith, Greenlee, Singh, Kraemer, & Hennig, 1998) and

portions of area IP. Area MT responds well to coherent versus random motion, suggesting that it is implicated in the perception of global motion (Smith, Wall, Williams, & Singh, 2006; Morrone et al., 2000; Van Oostende, Sunaert, Van Hecke, Marchal, & Orban, 1997). Interestingly, MT also shows spatio-topicity in its response to motion, meaning it is selective in real-world rather than retinal coordinates (d'Avossa et al., 2007). Area V3A also differentiates coherent from random motion (Koyama et al., 2005; Braddick et al., 2001; Braddick, O'Brien, Wattam-Bell, Atkinson, & Turner, 2000; Cornette et al., 1998).

Periventricular white matter damage is a common cause of early brain injury in preterm infants with low gestational age and low birth weight, accounting for most of the neurological morbidity in preterm infants. The most severe form of this condition, cystic periventricular leukomalacia (PVL), consists of a focal necrosis of variable severity at the level of deep white matter, surrounded by a more diffuse and milder injury of the tissue mainly affecting oligodendrocytes precursors

(Volpe, 2001). This lesion typically involves the cortico-spinal tract at the level of the posterior part of the *corona radiata*, resulting in a motor impairment primarily affecting the lower limbs, diplegic cerebral palsy. In most cases, however, the damage also involves the geniculo-calcarine tracts that are in close proximity to the posterior horns of the lateral ventricles, giving rise to variable degrees of cerebral visual impairment.

The most common visual disorders in children with PVL are reduced acuity, visual field restriction, and oculomotor difficulties, particularly with saccades (Fedrizzi et al., 1998; Cioni et al., 1997) that may or may not be a consequence of damage to the optical radiation or to other cortico-cortical fiber connections. An association between PVL and impairment of object recognition has also been reported (van den Hout et al., 2004; Stiers et al., 2001; Stiers, De Cock, & Vandenbussche, 1998, 1999), which is significantly correlated to specific anatomical features, such as decreased volume of the peritrigonal white matter and thinning of the parieto-occipital white matter (Ito et al., 1996; Goto, Ota, Iai, Sugita, & Tanabe, 1994; Koeda & Takeshita, 1992). Recently, we have shown that the perception of flow motion in diplegic children with cystic PVL is impaired, both for translational and rotational flow motion (Guzzetta et al., submitted). However, the impairment is small (less than a factor of 2). During this study, we observed two

cases of PVL children, with similar anatomical lesions to the others in the sample, where motion perception was affected in a most bizarre way, with translation being consistently seen in the wrong direction. We report in detail one of these cases.

METHODS

Subjects

During the previous study (Guzzetta et al., submitted) of 16 PVL patients, two (G.B. and S.L.) were observed with completely abnormal motion perception (described in the Results section). However, their clinical characteristics were very similar to the rest of the sample reported in Guzzetta et al. (submitted). Of the two, G.B. was a particularly cooperative patient and was tested exhaustively. Patient S.L., unfortunately, was not very cooperative, was easily distracted, and soon lost interest in the task. As the testing was clearly causing stress, we felt ethically bound to stop testing. For S.L. we were able to demonstrate only the basic effect of inverted motion. Table 1 summarizes the clinical details of the two patients.

Psychophysics

Sensitivity for motion coherency was assessed by measuring coherence thresholds for perceiving circular, radial,

Table 1.

	Patient S.L.	Patient G.B.
Age at test (years)	10	16
Gestational age	32 weeks	29 weeks
Verbal IQ	normal	normal
Visual assessment		
Refractive errors	mild myopia	mild myopia
Acuity (Snellen)	20/100	20/20
Visual fields	normal	normal
Oculomotor function	dysmetric saccades	normal
Strabismus	convergent	absent
MRI findings		
Ventricular size	normal	bilateral mild enlargement
Periventricular gliosis	diffuse bilateral	diffuse bilateral
Periventricular white matter	bilateral reduction	bilateral reduction
Cysts	no	no
Subarachnoid space	normal	normal
Corpus callosum	mild posterior thinning	mild posterior thinning
Cortical gray matter	normal	normal
Neurological diagnosis	spastic diplegia	spastic diplegia

and translational (up–down, left–right, and diagonal) motion. The stimuli comprised 100 small dots (each 35 arc min), half black and half white, presented to subjects in a dimly lit room on a 17-in. Sony CRT monitor (50 cd/m^2), subtending $22° × 22°$ when viewed from a distance of 60 cm. A proportion of dots drifted coherently at a local speed of 10 deg/sec (limited lifetime of 10 frames, frame rate 75 Hz), whereas the remainder of dots (noise dots) were displayed at random positions each frame (see icons in Figure 1). For the majority of the testing, the coherent motion was either upward or downward (chosen at random) for the translation condition, clockwise or counterclockwise for the circular condition, and expansion or contraction for the radial motion (all dots had constant local speed in all conditions), viewed binocularly with a presentation time of 250 msec (some controls for monocular viewing were also collected). Motion coherency of the stimuli was varied from trial-to-trial using the QUEST algorithm (Watson & Pelli, 1983) by substituting a proportion of the points with random noise, and measuring percent correct over a range of noise levels to produce the psychometric functions such as those of Figure 1. Sensitivity was defined as the maximum proportion of noise that produced 75% correct direction discrimination, calculated off-line by fitting all data of a particular condition (from 27 to 90 trials) with cumulative Gaussian functions. No feedback was given to the children. G.B.'s parents were informed of the specific deficit of their son after the first 6 months, by which time most of the tests had been completed. G.B. was probably aware of his perceptual deficit during the eye movement testing and the driving simulation test (performed primarily to test his ability as a potential driver of a special vehicle for disabled people).

For the contrast sensitivity measurements, stimuli were generated by VSG framestore (Cambridge Research Systems) and displayed on the face of a Barco monitor at $512 × 512$ pixels resolution at 126 Hz frame rate, with mean luminance of 10 cd/m^2 and a viewing distance of 100 cm (the low luminance was chosen to allow measurements of contrast sensitivity for equiluminant gratings). Stimuli were sinusoidal gratings of various spatial frequencies and orientations, caused to drift upward or downward (horizontal gratings), or rightward or leftward (vertical gratings), behind a diamond mask (that minimized edge effects that can create spurious cues of drift direction). Subjects had to identify the direction of drifting in two-alterative forced-choice task (in a given session, direction was always horizontal or vertical). Stimuli were presented within a Gaussian temporal window, usually of time constant of 100 msec. Some testing was performed with a 300-msec Gaussian presentation, yielding no major differences. In one condition, we also determined detection thresholds by requiring subjects to discriminate the orientation (not the drift direction) of the drifting grating, 45° clockwise or counterclockwise from the vertical (behind a square mask). As with the coherence measurements, grating contrast was varied after each response of the observers, following the adaptive QUEST (Watson & Pelli, 1983) algorithm. Final thresholds were determined by fitting a cumulative Gaussian to the resultant probability of seeing curves (on logarithmic abscissa).

Grating acuity was tested using the Teller acuity cards (McDonald et al., 1985), with acuity defined as the finest stripe width of the grating for which the subject consistently responds. Visual field size was assessed using kinetic perimetry. During central fixation of a centrally positioned

Figure 1. Psychometric functions (percent correct discriminations as a function of percent noise) for patient G.B. and an age-matched control P.G. for translational, radial, and circular motion. Although the psychometric functions for circular and radial motion are normal psychometric functions, going from perfect performance for low levels of noise to chance behavior at high levels, those for translational motion are quite different, running in the other direction, from 0% performance to chance. G.B. consistently saw the motion in the wrong direction, with about the same noise threshold as that for seeing circular and radial motion in the right direction (about 5%). The icons at the left illustrate the type of motion.
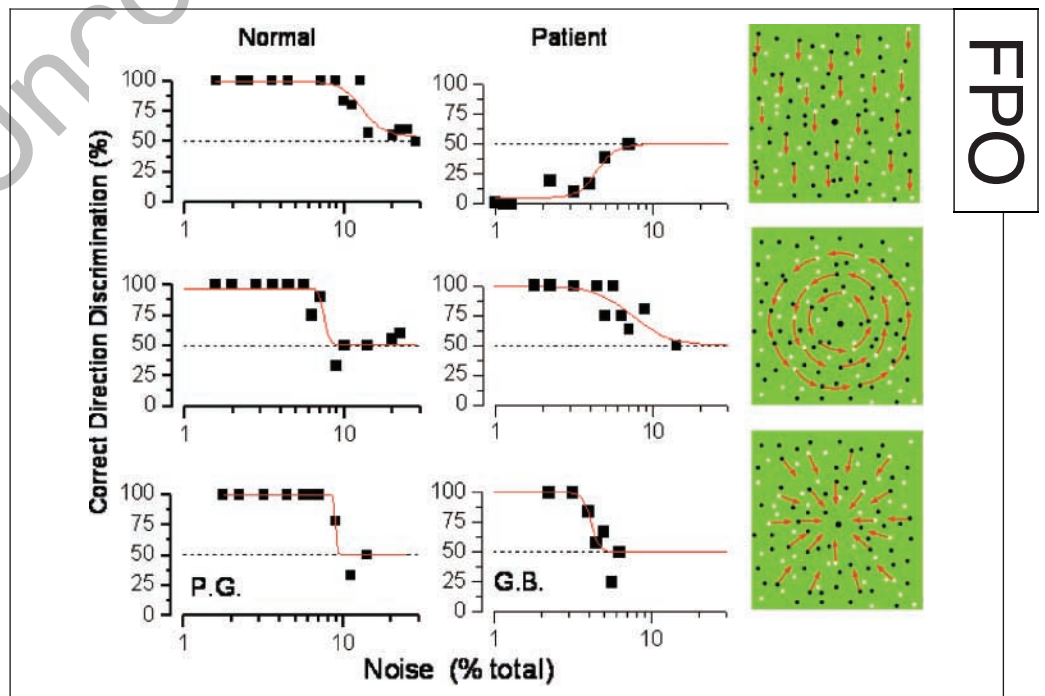
white ball, an identical target is moved from the periphery toward the fixation point along one arc of the perimeter. Eye and head movements toward the peripheral ball are used to estimate the outline of the visual field.

Eye movements were measured with an infrared sensor (ASL model 504) at a sampling frequency of 60 Hz. For the optokinetic nystagmus (OKN) measurements, the subject observed a high contrast drifting grating or a uniform field of white random dots drifting across a black background on a large television screen (50° × 70°, 60 Hz interlaced), with the head restrained with a comfortable head rest. The eye positions were calibrated on nine positions before the recording, and the calibration was repeated at the end of the recording session. The horizontal and vertical eye position signals were analyzed using the software provided by the ASL.

Strabismus was tested by examining symmetry of the corneal light reflex and by the cover test. Visual attention was scored according to a global qualitative evaluation of visual behavior during the entire duration of the assessment, in particular, of the oculomotor tasks.

Functional Magnetic Resonance Imaging Methods

Blood oxygenation level-dependent (BOLD) responses were acquired by a 1.5-T General Electric LX Signa Horizon System (GE, Milwaukee, USA), equipped with echo-speed gradient coil and amplifier hardware, using a standard quadrature head coil. Activation images were acquired using echo-planar imaging (EPI) gradient-recalled echo sequence (TR/TE/flip angle = 3 sec/50 msec/90°, FOV = 280 × 210 mm, matrix = 128 × 128, acquisition time: 3 min 12 sec). Volumes consisted in 18 contiguous 4-mm-thick axial slices, covering from the inferior temporal–occipital edge to the middle parietal region (from about z −28 to 45 mm), acquired every 3 sec. Time-course series of 64 images for each volume were collected in the 6 epochs. The first epoch lasted 12 sec more to allow the signal to stabilize and this initial period was eliminated from any successive analysis. An additional set of anatomical high-resolution 3-D FastSPGR dataset (TR/TE/flip angle = 150 msec/2.3 msec/120°; RBW = 12.8 kHz; FOV = 280 × 280 mm, matrix = 256 × 256; isotropic dimension: 1.1 mm, NEX:2; acquisition time: 12 min 26 sec), was acquired in order to generate a three-dimensional whole-brain reconstruction and a bicommissural axial projection to estimate the anatomical Talairach and Tournoux (1988) coordinates. For generating a statistical map of the BOLD response, Brain Voyager 2000 4.6 software package (Max-Planck Society, Germany and Brain Innovation, Maastricht, the Netherlands) was used. All volumes from each subject were adjusted with the application of rigid body transforms for residual motion-related signal changes. Functional data were smoothed spatially (Gaussian kernel with a 4-mm full width at half maximum) but not temporally. Statistical activation maps were obtained using cross-correlation or General Linear Model analysis, with thresholding at $p < .0022$ with a cluster size limit of two voxels. EPI images were coregistered with the 3-D anatomical data in order to define the Talairach–Tournoux coordinates.

The stimuli were random-dot kinematograms, similar to those used to measure coherence sensitivity (50 dots, 300 msec lifetime, 1° diameter dot size). Three types of coherent motion were used: translation, rotation (both inverting direction every 2 sec), or flow fields that changed gradually in 2 sec from pure expansion, to inward spiral, clockwise rotation, spiral, contraction, and so on. The dots moved along trajectories with a constant local speed of 7 deg/sec both for the coherent and the noise stimuli (Morrone et al., 2000). Stimuli were presented on LCD goggles (Resonance Technology) with a visual field of 22° × 30° and a luminance of about 30 cd/m². The resolution of the display was 600 × 800 pixels with a refresh rate of 60 Hz.

The research project was approved by the Ethical Committee of the Stella Maris Scientific Institute. Informed consent was obtained from all parents and from the children.

RESULTS

Seeing Reversed Motion

Figure 1 reports psychometric functions for discriminating the direction of global motion along a translational, circular, or radial trajectory for subject G.B. and an age-matched control (P.G.). In all cases, the measurements were forced-choice, with subjects discriminating upward from downward motion, clockwise from counterclockwise motion, or expansion from contraction (radial motion). The functions of the age-matched control were all orderly, varying monotonically from perfect performance at high coherence levels to chance (50%) at low levels.

For radial and circular motion, G.B.'s psychometric functions are very similar to those of the control, going from perfect performance for low levels of noise to chance behavior at high levels. However, the results for translational motion are spectacularly different: At high noise levels, performance was at chance, but at low noise levels, performance falls *below* chance to 0% correct, *perfectly incorrect discrimination*. In other words, G.B. consistently saw the motion in the wrong direction. Interestingly, the noise threshold for seeing translational motion in the wrong direction (the 25% correct point, corresponding to 5% noise) was very similar to that for seeing circular and radial motion in the right direction, and the form of the psychometric function was similar to the other two. This value was also very similar to average sensitivity for discriminating translational motion observed with the same techniques in a sample of age-matched PVL children (7%: Guzzetta et al., submitted), and not much worse than that for age-matched controls (∼10%).
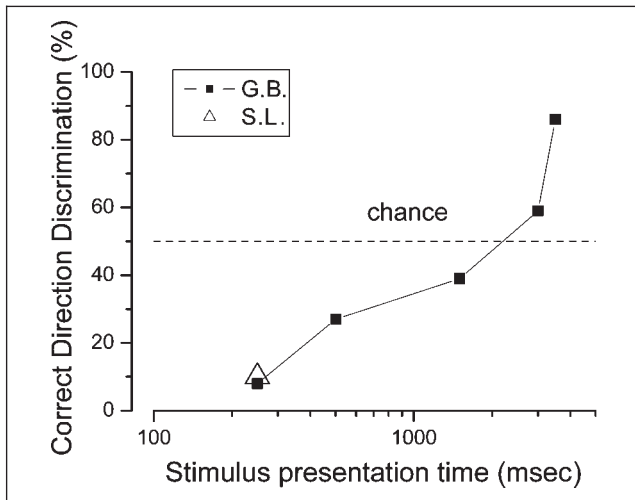
Figure 2. Discrimination performance as a function of stimulus duration. Discrimination ''improved'' systematically with stimulus duration, from almost perfectly incorrect at 250 msec, to 82% correct at 4 sec presentations. The squares report data from G.B., the triangle from S.L.

Patient S.L. was less collaborative and soon lost interest in the task. However, we did measure percentage correct for 100% coherence and 250 msec presentation time for translation (shown in Figure 2 by the triangle), and to obtain a threshold for circular motion (5.8, similar to the average PVL performance). G.B. was possible to study extensively. Figure 2 reports percent correct judgments for 100% coherence as a function of stimulus duration. For presentation times of 250 msec (the duration used for Figure 1), discrimination was almost perfectly incorrect for both subjects. At longer presentation times, however, performance for G.B. became less consistently incorrect. At 4-sec exposure durations, the tendency inverted and performance reached 82% correct. However, careful observation of the patient and subsequent debriefing revealed that this improvement at very long durations was not so much due to improved perception, as to clever deduction. G.B. observed the top and the bottom of the screen to see where the dots were disappearing. This was an effective strategy only when the presentations were long enough to see enough disappearances to deduce direction, and even then it was not perfect.

Using left–right or diagonal translation, or presenting the stimuli monocularly, did not change significantly the effect. Also, changing the size of the stimulus by changing viewing distance (from 40 cm to 4 m), or halving or doubling the velocity, did not change the inversion effect. The effect was robust over a wide range of stimuli.

Sinusoidal Gratings

We next measured motion discrimination for sinusoidal gratings of various spatial frequencies to see whether the motion inversion generalized to narrow-band stimuli

with no added noise. Interestingly, G.B. reported no inversion of direction for sinusoidal gratings, under any conditions. Figure 3 shows contrast sensitivity for motion discrimination of gratings drifting at 3 Hz, as a function of spatial frequency for G.B. (filled diamonds) and an age-matched control (open circles). At relatively low spatial frequencies (1 cycle/deg), G.B.'s performance was similar to the normal, correctly perceiving motion direction with contrast sensitivity of 200 (0.5% contrast). However, performance declined rapidly with spatial frequency, falling to 1 at 4 cycles/deg (while the sensitivity of the control remained around 200). The square and triangular symbols show results for gratings drifting at 6 and 15 Hz (respectively). The pattern is similar as for 3 Hz: good sensitivity at 1 cycle/deg, but none at 6 cycles/deg. However, under none of these conditions did G.B. see a drift in the wrong direction, as with the random-dot kinematograms. Interestingly, the deficit at high spatial frequencies was specific to judging motion direction: G.B. had good contrast sensitivity if he had to report the orientation of a drifting grating instead of the direction of motion (open pentagon symbols with dashed line).

Eye Movements

The poor performance in motion perception predicts that eye-tracking movements will also be compromised.
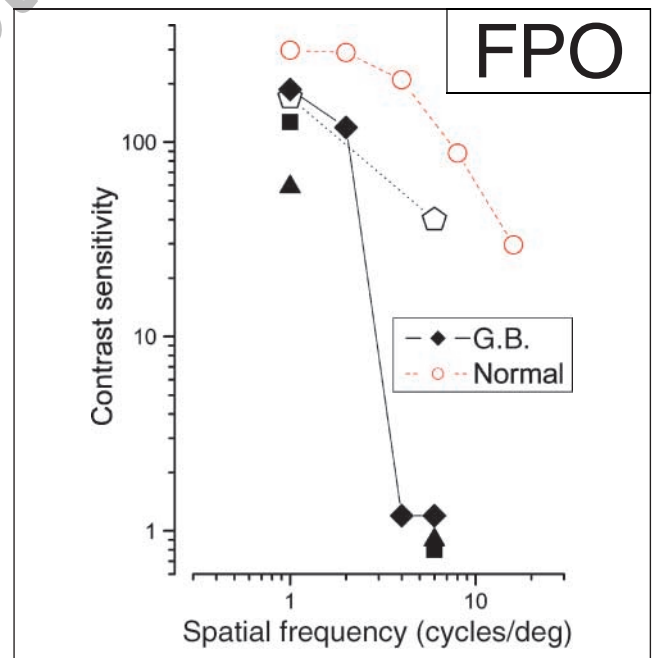
Figure 3. Contrast sensitivity for seeing the direction of gratings as a function of spatial frequency. The filled diamonds refer to G.B. and the open circles to an age-matched control. The gray square and triangle show results for G.B. at 6 and 15 Hz, respectively. The open pentagons show the sensitivity to discriminate orientation of the grating, not direction of motion. The temporal frequency for all other data points was 3 Hz. Sensitivity of less than unity means that performance did not reach criterion at maximum contrast (1).
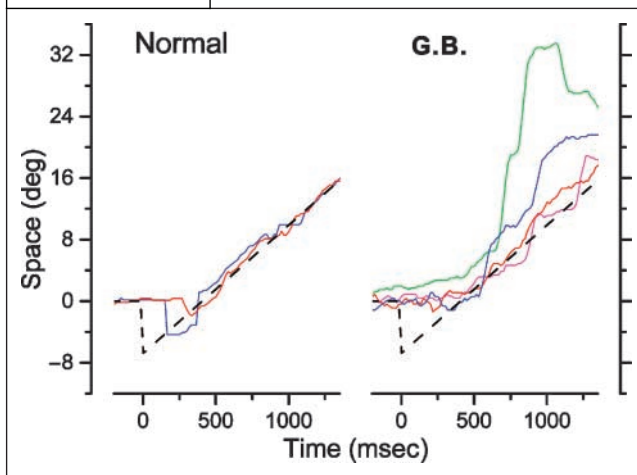
Figure 4. Examples of tracking records for a jump-ramp target (dot size 1°) for G.B. (right) and an age-matched control (left). The traces of the control are typical, showing a saccade in the direction of the jump, followed by smooth tracking movement matched to the drift speed. The traces for G.B. are completely different, with no initial saccade in the direction of the jump and very long latencies for initiation of pursuit tracking. Tracking was extremely inaccurate for G.B., more a series of rapid, saccadic-like movements keeping up roughly with the target.

Figure 4 shows example tracking records for a jump-ramp target (Newsome, Wurtz, Duersteler, & Mikami, 1985) for an age-matched control (left) and for G.B. (right). The typical performance, illustrated by the traces on the left, is for subjects to saccade in the direction of the jump, followed by smooth tracking movement matched to the speed of the drifting dot. Latencies for commencing the pursuit movement, often taken as an index of the time necessary to process motion information, ranged from 200 to 300 msec. Sometimes, a small corrective saccade was necessary to refoveate the target, but the tracking generally kept the target within about a degree of the fovea, and nearly stationary on the retina (see blue trace).

G.B.'s behavior was completely different. There was no initial saccade in the direction of the jump, and the latency for initiation of pursuit tracking was excessively long, around 500 msec. Once the tracking had started, it was extremely inaccurate, more a series of rapid, saccadic-like movements roughly keeping step with the target.

Although smooth pursuit movements were severely impaired for G.B., OKN was perfectly normal. Figure 5 shows responses to observing a 50° × 70° grating drifting at 10 deg/sec. The following responses to the drifting wide-field stimuli were reasonably normal, both in the slow phase (lasting up to a second) and in the rapid phase. The only difference was that his latency to commence OKN was often slower than that for the controls. Clearly, the impediment for tracking is selective to small target, reflecting a perceptual rather than a motor problem.

Driving Simulation

In order to assess G.B.'s perceptual abilities in a semi-natural situation (and to advise his parents on his capacity to drive a motorized vehicle), we tested him with a driving simulation video game based on a straight track with perpendicular interesting streets, projected on a wide screen (100° × 70°). The requirements of the game were navigation of the vehicle, and stopping for different visual stimuli, both moving (car and pedestrian) and stationary (such as traffic light). The motion in the scenes was mainly peripheral, with the focus of the flow in the center of the track. Although no age-normalized data exist on this specific video game, G.B. showed a peculiar behavioral pattern. He was good at driving the car through the street path at various simulated speeds, but showed problems in stopping the car without swerving when a moving obstacle crossed the street, suggesting that he apprehended the impending collision with the moving object too late. The same reaction difficulty was apparent with changing streetlights. However, this difficulty was not related to a mere delay of reaction times, as demonstrated by the fast arresting response he showed in relation to nonmoving stimuli.

## Functional Magnetic Resonance Imaging Responses

To gain further insight into the cortical areas compromised, we measured the BOLD activity of G.B. and an age-matched control, in response to translating and rotating stimuli (compared with blank controls). Figure 6 shows responses in the primary and secondary visual cortex, and two putative motion areas V3 and MT complex (indicated by green arrow). For both translational and circular motions, there was a strong response in V1/V2 in both G.B. and the control. The response in V3 and V3A was also prominent for G.B. and the control, although a clear differentiation of retinotopic areas is difficult without topographic mapping, particularly in a pathological brain where Talairach localization is reduced. A clear difference in activity between the control and G.B. was evident along the inferior temporal sulcus. For G.B., however, MT+ was activated only by circular motion, whereas both types of motion activated a similar located area for the control. As previously observed, radial flow activated a more anterior region with respect to the inferior temporal sulcus (Smith et al., 2006; Morrone et al., 2000) in the normal control. This result is surprising given that the motion is contrasted with a blank stimulus, and that the response of primary areas is quite normal.

To study more closely the motion-specific response of G.B., we measured BOLD activity when circular or translational motion was alternated with locally matched random motion (Figure 7). Circular motion, which alternated direction every 2 sec, elicited strong BOLD activity in the MT+ area (red-labeled activation) that is located along all the inferior temporal sulcus (from $z = 1$

Figure 5. Optic–kinetic nystagmus (OKN) eye movements of G.B. (lower) and control (upper) while observing a 50° × 70° grating drifting rightward at 10 deg/sec. The traces for G.B. are similar to those of the control, showing clear periods of tracking near the drift speed, followed by corrective controls.
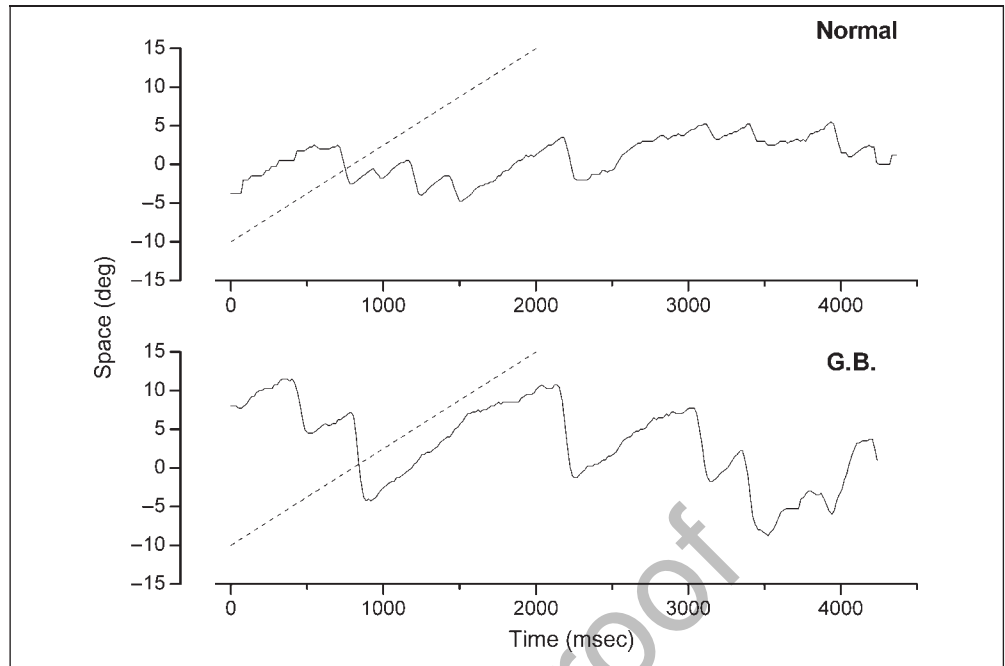
Figure 6. BOLD responses in the primary and secondary visual cortex, and two putative motion areas V3 and MT complex (indicated by green arrow). For both translational and circular motion, there was a strong response in V1/V2 in both G.B. and the control. The response in V3 (−**38,** −**85,** +**8**) for G.B. is also prominent. However, MT+ was activated only by circular motion for G.B. (−**48,** −**62, 1** and **55,** −**65, 14**), whereas both forms of motion activated the area for the control.
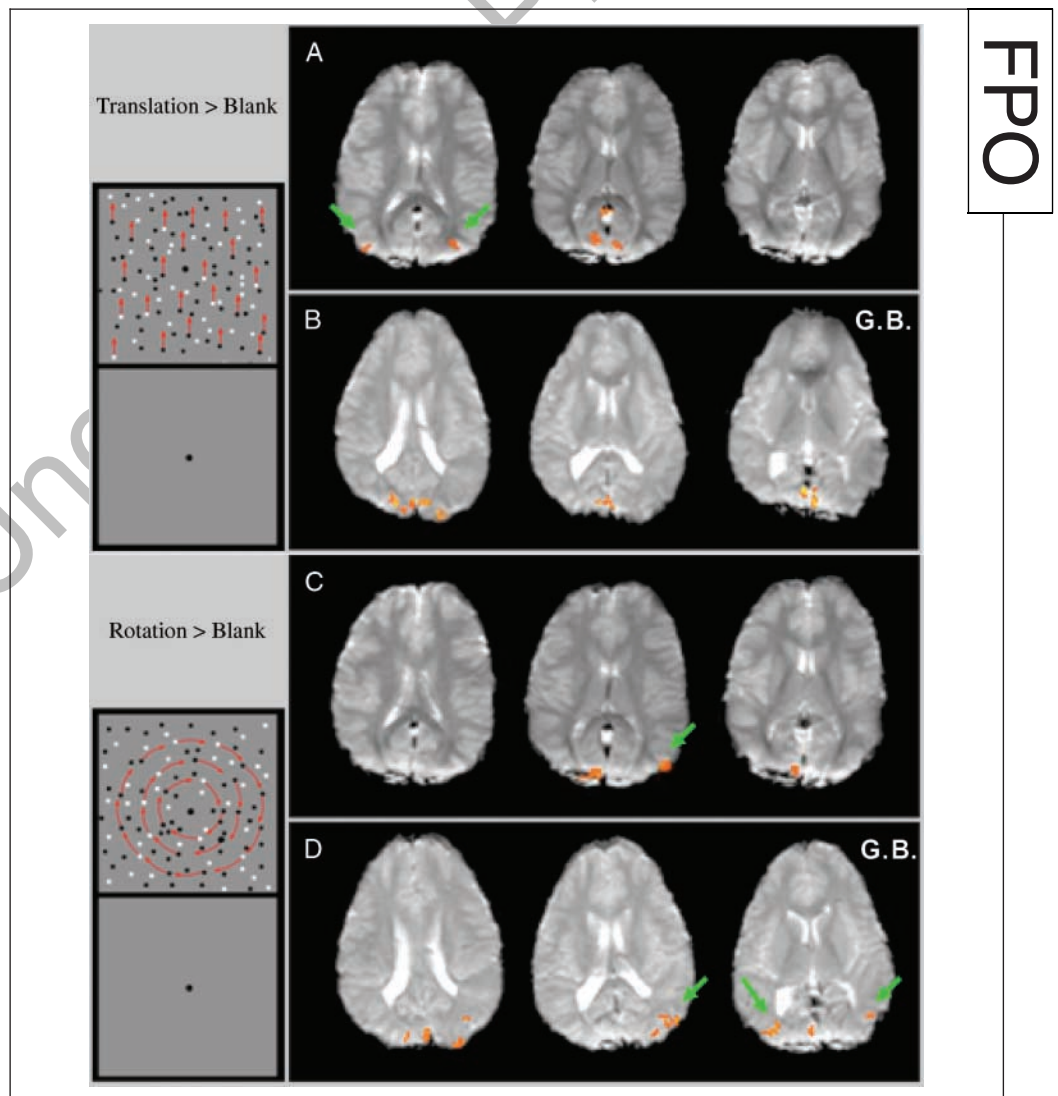
to about $z = 14$), both in the left and right hemispheres. Translational motion produced a smaller response than noise in these areas. Interestingly, the major area activated is located in a slightly different position along the sulcus that crosses the response to rotation. There was also a weak negative signal (correlated with noise rather than with coherent translation) in areas V3 and V1/V2 (not shown), suggesting that the locus of the deficit might precede MT. The rotation versus noise produced a reliable and positive response in V3 and V3A, but not primary areas (consistent with previous reports: Koyama et al., 2005). A preference for incoherent motion in V1/V2 has been previously observed in normal subjects, but was related to a noise comprising several velocities, due to the random refresh at each frame (Braddick et al., 2001) and to a low-density stimuli (McKeefry, Watson, Frackowiak, Fong, & Zeki, 1997). The response of normal subjects to the same translation versus noise stimuli used for G.B. never produced a negative response in V1, V2, V3, and V3A areas.

Modeling the Effect

The systematic inversion of perceived motion direction suggests that the system is aliasing the motion signal. A familiar example of aliasing is the so-called wagon wheel effect, where the spoked wheels in a Western movie seem to move backward when they reach a certain speed. This results from the periodic nature of the spokes of the rotating wheels, so if one spoke moves more than halfway toward the position of the next spoke in the time of one frame, it will be paired with the successive spoke, causing the direction of motion to invert (Roget, 1825). Technically, the inversion is known as *aliasing*, resulting from the fact that the rate of sampling by the filming technique is less than twice that of the repetition rate of the spokes, which is the minimum frequency necessary for vertical sampling (the *Nyquist* frequency).

What could cause the aliasing in this case? The undersampling could result from damage to the optic radiation, damaging the inputs to the motion-selective neurons. In this section, we attempt to simulate the effects of sparsely distributed input to the motion detectors. The flow of the model is illustrated by the center panels of Figure 8. There are four separate stages: an initial low-pass filter, spatial sampling, a second low-pass filter, and a final evaluation of motion direction. The initial filter essentially results from the optics and the finite size of the receptive fields of retinal neurons and the center–peripheral antagonism of the receptive field. The sampling stage assumes that the receptive fields that constitute the inputs to the motion-selective cells form an irregular lattice, each separated from its neighbor by an average distance that will be the inverse of the sampling rate (the minimum sampling distance was $0.11°$ which, for a 500-msec lifetime and a 1 deg/sec velocity, corresponds to a maximum of 4 samples per dot trajectory). The second filter stage relates to the spatial and temporal tuning of the ensemble of cortical motion detectors (or other neurons downstream of them) that receive the sampled information.

Figure 8 illustrates the effect of each stage of the model on the stimulus (upper panels) and its Fourier transform

Figure 7. BOLD activity of G.B., in response to circular (inverting direction every 2 sec) and translational motion, alternated with locally matched random motion. Circular motion produced strong BOLD in the low MT+ area (areas labeled in red for positive correlation, $z = 3.1$), but translational motion produced a smaller response than random noise with matched speed (area labeled in blue and corresponding to $z = -3.1$). The focus of the positive activity in response to the circular motion versus noise extended from (55, −65, 14) to (48, −60, 8) and from (−48, −60, 8) to (−48, −62, 1), whereas the focus of the negative response to translation versus noise was slightly shifted.
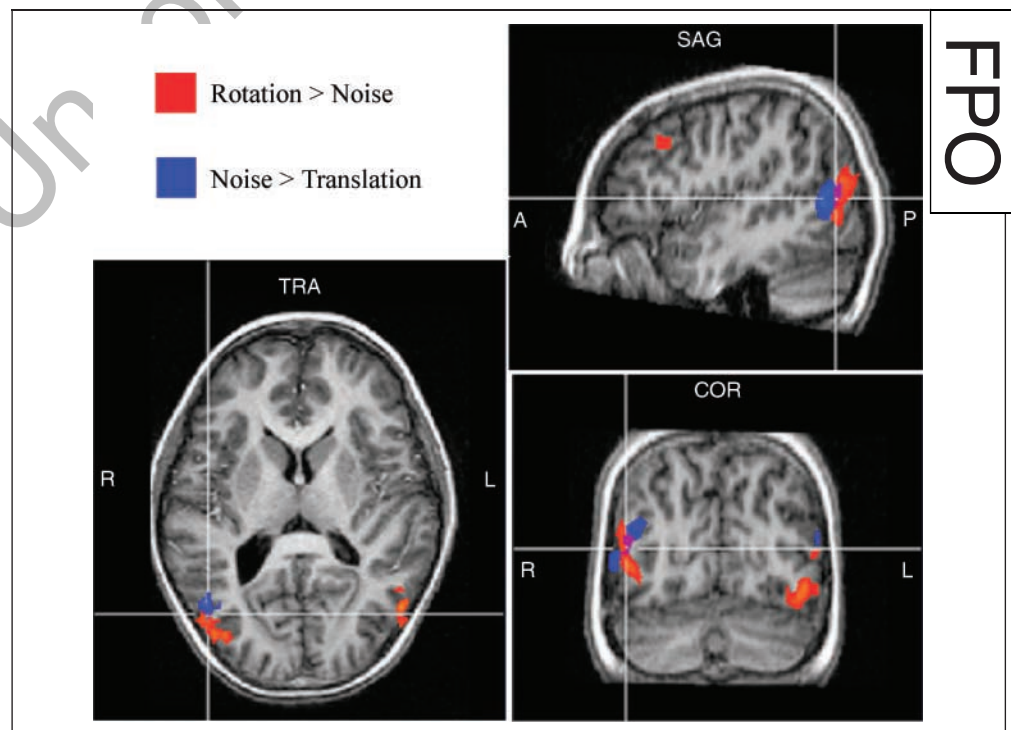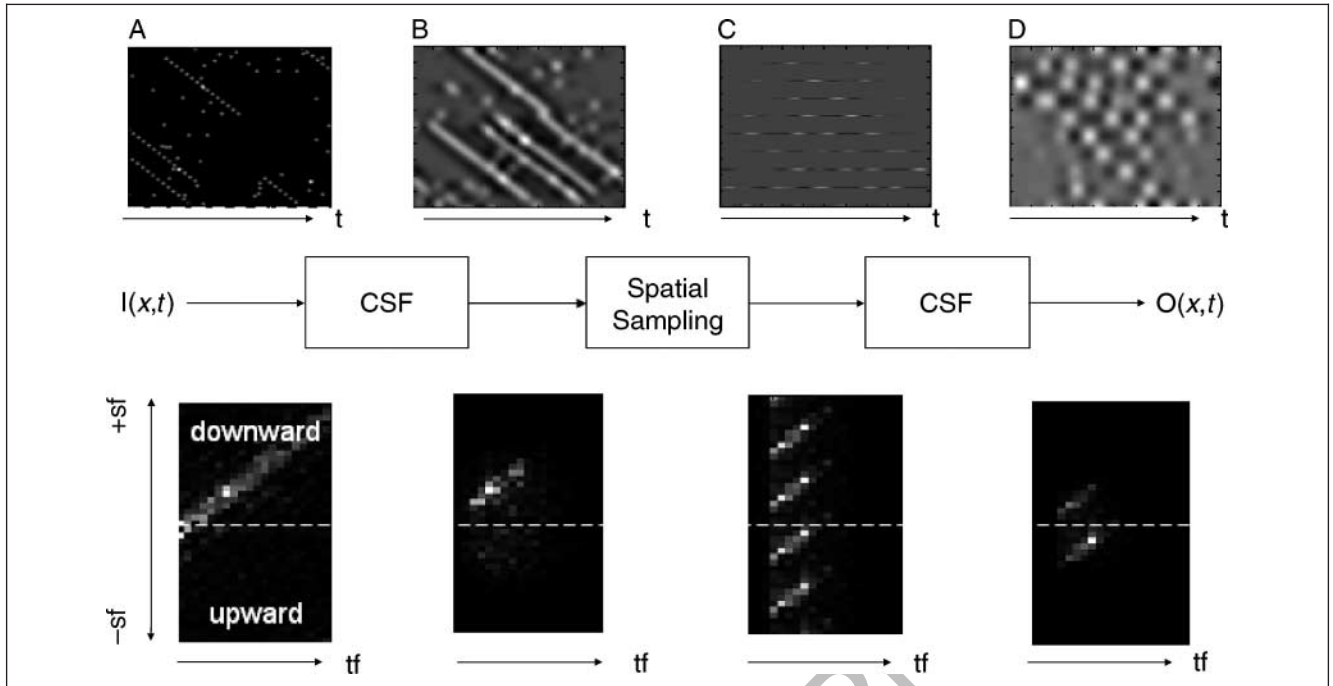
Figure 8. The center panels illustrate the four separate stages to the model: initial low-pass filter, spatial sampling, second low-pass filter, and a final evaluation of motion direction. The upper panels show the stimulus and the lower panels its Fourier transform. (A) The vertically translating stimulus (ignoring the horizontal dimension). The real component of the Fourier transform of the stimulus is shown underneath, with most energy falling in the upper quadrant, indicating that the motion was predominantly downward. (B) The image after spatio-temporal filtering by the retina, and its Fourier transform. (C) The result of multiplying this image by the sampling matrix, that would correspond to the sparsely positioned neurons that constitute the input to the cortical motion detectors, and its corresponding Fourier transform. There is now considerable energy in the lower quadrant, implying upward motion. After further spatio-temporal filtering (D), the energy is dominant in the lower quadrants, implying that upward motion would be seen. The filters are given by:

$$f(y,t) = \left(e^{\left(\frac{-y^2}{2\sigma_{SH}^2}\right)} - 0.5 e^{\left(\frac{-y^2}{2\sigma_{SL}^2}\right)} \right) \left(e^{\left(\frac{-t^2}{2\sigma_{TH}^2}\right)} - e^{\left(\frac{-t^2}{2\sigma_{TL}^2}\right)} \right)$$
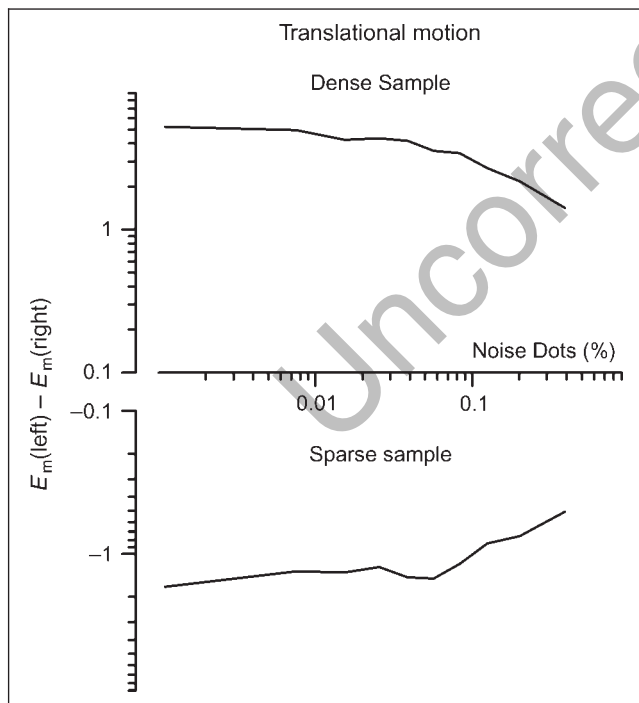
where for the initial filter $\sigma_{SH} = 5.4$ cycles/deg, $\sigma_{SL} = 2.25$ cycles/deg, $\sigma_{TH} = 6.75$ cycles/deg, $\sigma_{TL} = 3.5$ cycles/deg. For the second-stage filter, only the low-pass spatial function was present, with $\sigma_{SH} = 4.5$ cycles/deg, and the other parameters of the temporal functions remained the same. Sampling was at $0.11°$, lifetime 500 msec and velocity 1 deg/sec (similar results were obtained over a factor of two range of velocities).

(lower panels). We consider only the vertical spatial direction (represented on the ordinate) and time (on the abscissa). With this representation, the translating stimuli follow short downward trajectories equal to their limited lifetime, shown by the runs of dots at $45°$ in Figure 8A. The few isolated dots are the noise dots, repositioned to a new random position each frame. The real component of the Fourier transform of the stimulus is shown underneath. Most energy falls in the upper quadrant, indicating that the motion was predominantly downward. Figure 8B shows the image after spatio-temporal filtering by the retina (details in caption), which has the effect of smoothing the image in space–time. Figure 8C and its Fourier transform shows the result of multiplying this image multiplied by the sampling matrix, which would correspond to the sparsely positioned cortical motion detectors. There is now considerable energy in the lower quadrant (upward motion), nearly balanced with the downward
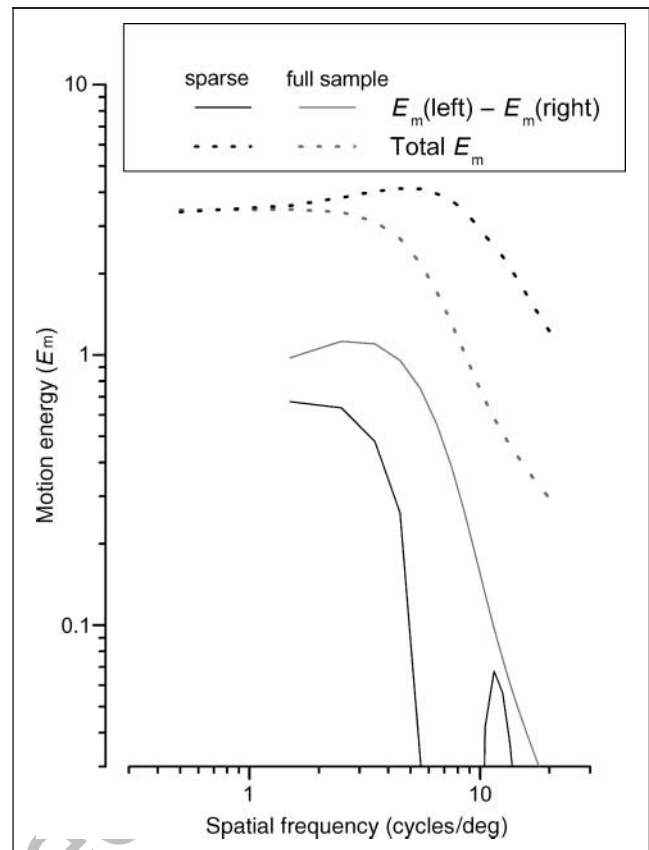
motion. After further spatio-temporal filtering (Figure 8D: probably imposed at cortical level), much of the energy in the upper quadrant is removed so that the lower quadrant becomes dominant, implying that upward motion would be seen. This second-stage filtering simulates the action of the spatio-temporal selectivity of the ensemble of motion detectors. The shape of this secondary filter is crucial in simulating the data: A second-stage spatial filter that is band-pass rather than low-pass, or a low-pass with a larger bandwidth, would eliminate the bias toward upward motion (see Discussion). Indeed, the inversion effect is replicated because the peak of the aliasing spectra comes close to the low spatial frequency for the downward motion, whereas the peak for the upward motion is filtered out by the low spatial frequency selectivity of the motion detector. In this implementation, the motion was sampled regularly. However, similar results were obtained with random sampling, provided that there was a

minimum distance between sampling and that it was in the range of aliasing (maximum allowed for this motion parameter is 0.08°).

To predict the perceived direction of motion, we assume a subtractive stage, typical of many motion models (Adelson & Bergen, 1985; Reichardt, 1961) that judge the direction from the difference of the overall energy in the two quadrants. The model was implemented in the Fourier domain, measuring all the energy (square root of the integral of the power) that belongs to the first (upward motion) and second (downward motion) quadrants. For simplicity, no normalization stage (e.g., Georgeson & Scott-Samuel, 1999) was introduced, as we observed that this operation did not alter the simulation very much, given that total energy changes only slightly with sampling frequency when normalized for number of samples. Figure 9 shows the result of the model as a function of motion coherence level, for sparse and dense (near continuous) sampling. For a wide range of coherence levels, the sparse sampling predicts motion in the reversed direction. At very low coherence levels, the difference of energy in the reversed direction decreases, but never inverts. Interestingly, the amount of motion energy for the sparse sampling falls at about the same rate as that for the dense sampling, predicting that the

Figure 10. Directed motion energy for drifting sinusoidal gratings as a function of spatial frequency, for sparse (0.11°, gray lines) and near-continuous (0.005°, dashed lines) sampling. The sparse sampling predicts veridical motion for spatial frequencies below about 5 cycles/deg, with a rebound of inverted motion around 10–12 cycles/deg. However, this rebound is of low amplitude, probably below threshold. Velocity was kept constant at 1 deg/sec.

Figure 9. Output of the motion model with sparse and dense sampling, as a function of motion coherence level. The sparse sampling always produces a prevalence of inverted energy. In both cases, the energy differences fall off with coherence at a similar rate, indicating that thresholds should be similar. Each point at each coherence is an average of 80 different new stimuli. The sparse sampling of the image was 0.11°, the dense 0.005°; stimulus velocity 1 deg/cycle, lifetime 500 msec, average density of 0.1 dots/deg^2.

inverted thresholds for sparse sampling should be similar to the veridical thresholds for dense sampling (as is observed with G.B.). Similar results were obtained decreasing velocity by a factor of 3 or increasing it by a factor of 2. The critical parameters to achieve this simulation are minimum spatial sampling (a less severe sampling would not produce the inversion) and second-stage filtering that boasts selectively the spurious low spatial frequencies and high temporal frequencies in the wrong direction.

We also ran the prediction for sinusoidal gratings, as a function of spatial frequency, for sparse and continuous sampling (Figure 10). The sparse sampling predicts veridical motion for spatial frequencies below about 5 cycles/deg, with a rebound of inverted motion around 10–12 cycles/deg. However, this rebound is of low amplitude, probably below threshold.

DISCUSSION

We have described two PVL patients that not only had severely impaired motion perception but also consis-

tently and reliably saw motion in the opposite direction. This occurred only for translational motion, not for circular or radial motion, and only for random-dot kinematograms, not for sinusoidal gratings. Interestingly, the sensitivity threshold for seeing reversed translational motion in one patient was similar to that for seeing correct rotational and radial motion, and similar to that for seeing correct translation in other PVL patients and typically developed children (Guzzetta et al., submitted). With sinusoidal gratings, contrast sensitivity for direction discrimination plummeted rapidly to zero at 3 cycles/deg (a relatively low spatial frequency), but the direction was never perceived inverted. Orientation sensitivity for gratings drifting at the same temporal frequency was well within the normal range, showing that, even for sinusoidal gratings, the deficit was specific for motion discrimination.

Selective impairment of contrast sensitivity for direction discrimination has been observed in adult patients with middle temporal lesions (Hess, Baker, & Zihl, 1989). The same patients also show a clear deficit for coherence thresholds, in good agreement with electrophysiological and functional magnetic resonance imaging studies that implicate the MT–MST complex in the elaboration of motion signals to mediate the perceptual thresholds (Rees et al., 2000; Britten et al., 1996). However, no case of perceptual inversion of motion direction has ever been reported, either in monkeys with experimental lesions (Pasternak & Merigan, 1994) or in lesioned patients (Vaina, Cowey, Jakab, & Kikinis, 2005; Vaina, Cowey, & Kennedy, 1999). In our patient G.B., translational motion never activated the MT complex, even when contrasted with blank stimuli. When contrasted with random noise, there was a clear response in the contralateral hemisphere along the region that is usually called MT (see Smith et al., 2006), but the response was negative (stronger for random noise than coherent motion). A similar preference for noise was observed in occipital areas within BA 17, 18 and 19. Although a preference for random noise has been observed previously in the literature (Braddick et al., 2001; McKeefry et al., 1997), it usually occurs with a noise that comprises several velocities, due to random refreshment of each frame or to a low density of the random dots. The noise used here to contrast the coherent translation has the same local speed and the same limited lifetime of the coherent motion dot. In our laboratory, contrasting these motions produces a null or weak response in the calcarine cortex and a positive response in V3 and V3A (see also Koyama et al., 2005). The preference for noise over coherent translation is consistent with a perceptual deficit for translation, and also with the existence of the specificity within the MT complex for this type of motion.

This result would indicate that the signal elicited by coherent motion does not reach MT, or that it is heavily reduced. On the other hand, the activation generated by rotation or radial flow seems to be normal both for the occipital cortex (Koyama et al., 2005) and the MT complex. The segregation of the two regions along the inferior temporal sulcus also seems normal, with the translation selective area more dorsal and posterior, crossing at a certain point along the sulcus as observed in detail by Smith et al. (2006). Radial and rotational flow motions are analyzed by different neuronal mechanisms from those for translational motion, with very large neuronal receptive fields that summate local motion signals over an extensive area (Burr, Morrone, & Vaina, 1998; Morrone, Burr, & Vaina, 1995; Duffy & Wurtz, 1991). That G.B.'s perception and BOLD activation are compromised for translational but not for flow motion reinforces the evidence for separate cortical subareas in MT, with independent function and different vulnerability to damage.

The eye-movement results are also consistent with a central site of the damage. The subject had great difficulty in pursuing an isolated target, presumably because he cannot see the motion. However, large-field stimulation with low spatial frequency gratings elicits near-normal OKN. Given that the cortical circuitry controlling pursuit and OKN are thought to overlap to a great extent (but not completely), it is reasonable to believe that the deficit is in the perceptual analysis and not in the motor control of the eye movement. Lesions in MT in monkey induce a strong but transient deficit of pursuit eye movement, and also erratic and delayed "catch-up" saccades to refoveate during pursuit (Newsome et al., 1985). The inability to perceive correctly direction of motion seems not to be related to the view of field, with the same impairment observed with a single dot and the 20° random dot display used for the direction discrimination task.

The anatomical lesions and the other neuropsychological and neurological tests for the two patients reported here were very similar to those of other PVL patients reported by our laboratory (Guzzetta et al., submitted). Their lesions were absolutely typical for PVL patients, and even careful neuro-radiological examination did not reveal additional subcortical or cortical lesions. One possibility is that the optic radiations of the two patients were more impaired than that of others, and that this was not anatomically resolvable. Perhaps the impairment is predominantly to the magnocellular afference, thought to be more vulnerable to compression damage (Tassinari, Marzi, Lee, Di Lollo, & Campara, 1999). The magnocellular pathway is clearly implicated in motion perception, whereas the parvocellular pathway is thought to be more important for visual acuity and form. This would be consistent with the fact that spatial acuity and contrast sensitivity were normal for G.B., and the fact that previous research has shown that PVL patients tend to show a motion rather than a form perception deficit (Gunn et al., 2002).

The bizarre inversion of motion direction suggests that the system is somehow *aliasing* the motion signal,

in a form of "wagon wheel effect," where the spoked wheels in a Western movie seem to move backward when they reach a certain speed. This effect results from motion being sampled discretely rather than continuously, by a sampling technique such as cinematography or television. There has been some suggestion that a similar effect can occur without discrete sampling, implicating a sampling process in the brain (Purves, Paydarfar, & Andrews, 1996), but this idea has been effectively dismissed by controlled experiments (Kline, Holcombe, & Eagleman, 2004; Pakarian & Yasamy, 2003). It therefore seems more likely that the effect results from spatial rather than temporal undersampling, possibly a result of damage to the optic radiation. Figures 8, 9, and 10 show results of simulations predicting an inversion of motion direction by severe undersampling, in a way that could occur if many inputs to motion-selective neurons had been destroyed. The simulations predict the inversion of motion direction, and that the coherence thresholds for the inverted motion should be similar for those of veridical motion (with appropriate sampling). Sinusoidal gratings of low spatial frequency should be seen as veridical. However, the spatial sampling predicted that motion direction should not be discernable for frequencies higher than about 4 cycles/deg, as observed with GM. In theory, inverted motion may be seen in a very narrow band of spatial frequencies around 10 cycles/deg, but this would be very difficult to measure in practice, as the thresholds would be very high and the spatial frequency quite critical.

Why the reversed motion should occur only for translational motion and not for circular or radial motion is far from obvious. One point to note is that translational motion seems to be processed, at least in part, in different neural centers from radial motion (Morrone et al., 2000); these areas could have different properties that make them more vulnerable to undersampling. A crucial part of the model is the second-stage spatio-temporal filter that filters out much of the energy, leaving a surplus in the reverse direction. Changing the characteristics of this filter can have a large effect on the output: for example, broadening the spatial low-pass filter, or making it band-pass causes the output to be veridical rather than biased. If, for example, the areas that detect circular and radial motion had less severe low-pass filtering, then the aliasing would be less. At present, there are no data to confirm this suggestion, but it seems reasonable, given that very low spatial frequencies provide useful information for translation, but not for radial or rotational motion. Indeed, this could be a useful line to pursue in future research (in normal adults).

In conclusion, our results reinforce previous evidence that translational motion is processed by structures that are functionally, and probably anatomically distinct from those that process circular and radial motion. That PVL lesions can lead to undersampling of motion, and the paradoxical perception of inverted motion, provides important clues about the neural mechanisms that analyze motion in human.

REFERENCES

Adelson, E. H., & Bergen, J. R. (1985). Spatio-temporal energy models for the perception of motion. *Journal of the Optical Society of America, A2,* 284–299.

Braddick, O. J., O'Brien, J. M., Wattam-Bell, J., Atkinson, J., Hartley, T., & Turner, R. (2001). Brain areas sensitive to coherent visual motion. *Perception, 30,* 61–72.

Braddick, O. J., O'Brien, J. M., Wattam-Bell, J., Atkinson, J., & Turner, R. (2000). Form and motion coherence activate independent, but not dorsal/ventral segregated, networks in the human brain. *Current Biology, 10,* 731–734.

Britten, K. H., Newsome, W. T., Shadlen, M. N., Celebrini, S., & Movshon, J. A. (1996). A relationship between behavioral choice and the visual responses of neurons in macaque MT. *Visual Neuroscience, 13,* 87–100.

Burr, D. C., Morrone, M. C., & Vaina, L. (1998). Large receptive fields for optic flow direction in humans. *Vision Research, 38,* 1731–1743.

Cioni, G., Fazzi, B., Coluccini, M., Bartalena, L., Boldrini, A., & van Hof-van Duin, J. (1997). Cerebral visual impairment in preterm infants with periventricular leukomalacia. *Pediatric Neurology, 17,* 331–338.

Cornette, L., Dupont, P., Rosier, A., Sunaert, S., Van Hecke, P., Michiels, J., et al. (1998). Human brain regions involved in direction discrimination. *Journal of Neurophysiology, 79,* 2749–2765.

d'Avossa, G., Tosetti, M., Crespi, S., Biagi, L., Burr, D. C., & Morrone, M. C. (2007). Spatiotopic selectivity of BOLD responses to visual motion in human area MT. *Nature Neuroscience, 10,* 249–255.

Duffy, C. J., & Wurtz, R. H. (1991). Sensitivity of MST neurons to optic flow stimuli. II. Mechanisms of response selectivity revealed by small-field stimuli. *Journal of Neurophysiology, 65,* 1346–1359.

Fedrizzi, E., Anderloni, A., Bono, R., Bova, S., Farinotti, M., Inverno, M., et al. (1998). Eye-movement disorders and visual–perceptual impairment in diplegic children born preterm: A clinical evaluation. *Developmental Medicine & Child Neurology, 40,* 682–688.

Georgeson, M. A., & Scott-Samuel, N. E. (1999). Motion contrast: A new metric for direction discrimination. *Vision Research, 39,* 4393–4402.

Goto, M., Ota, R., Iai, M., Sugita, K., & Tanabe, Y. (1994). MRI changes and deficits of higher brain functions in preterm diplegia. *Acta Paediatrica, 83,* 506–511.

Gunn, A., Cory, E., Atkinson, J., Braddick, O., Wattam-Bell, J., Guzzetta, A., et al. (2002). Dorsal and ventral stream sensitivity in normal development and hemiplegia. *NeuroReport, 13,* 843–847.

Guzzetta, A., Tinelli, F., Del Viva, M., Bancale, A., Pascale, R. R., & Cioni, G. (submitted). Perception of motion in children with periventricular leukomalacia. *Neuropsycholgia*.

Heeger, D. J., Boynton, G. M., Demb, J. B., Seidemann, E., & Newsome, W. T. (1999). Motion opponency in visual cortex. *Journal of Neuroscience, 19,* 7162–7174.

Hess, R. H., Baker, C. L., Jr., & Zihl, J. (1989). The ''motion-blind'' patient: Low-level spatial and temporal filters. *Journal of Neuroscience, 9,* 1628–1640.

Ito, J., Saijo, H., Araki, A., Tanaka, H., Tasaki, T., Cho, K., et al. (1996). Assessment of visuoperceptual disturbance in children with spastic diplegia using measurements of the lateral ventricles on cerebral MRI. *Developmental Medicine & Child Neurology, 38,* 496–502.

Kline, K., Holcombe, A. O., & Eagleman, D. M. (2004). Illusory motion reversal is caused by rivalry, not by perceptual snapshots of the visual field. *Vision Research, 44,* 2653–2658.

Koeda, T., & Takeshita, K. (1992). Visuo-perceptual impairment and cerebral lesions in spastic diplegia with preterm birth. *Brain Development, 14,* 239–244.

Koyama, S., Sasaki, Y., Andersen, G. J., Tootell, R. B., Matsuura, M., & Watanabe, T. (2005). Separate processing of different global-motion structures in visual cortex is revealed by fMRI. *Current Biology, 15,* 2027–2032.

McDonald, M. A., Dobson, V., Sebris, S. L., Baitch, L., Varner, D., & Teller, D. (1985). The acuity card procedure: A rapid test of infant acuity. *Investigative Ophthalmology & Visual Science, 26,* 1158–1162.

McKeefry, D. J., Watson, J. D., Frackowiak, R. S., Fong, K., & Zeki, S. (1997). The activity in human areas V1/V2, V3, and V5 during the perception of coherent and incoherent motion. *Neuroimage, 5,* 1–12.

Morrone, M. C., Burr, D. C., & Vaina, L. (1995). Two stages of visual processing for radial and circular motion. *Nature, 376,* 507–509.

Morrone, M. C., Tosetti, M., Montanaro, D., Burr, D. C., Fiorentini, A., & Cioni, G. (2000). A cortical area that responds specifically to optic flow, revealed by function magnetic resonance imaging. *Nature Neuroscience, 3,* 1322–1328.

Newsome, W. T., Wurtz, R. H., Duersteler, M. R., & Mikami, A. (1985). Deficits in visual motion processing following ibotenic acid lesions of the middle temporal visual area of the macaque monkey. *Journal of Neuroscience, 5,* 825–840.

Pakarian, P., & Yasamy, M. T. (2003). Wagon-wheel illusion under steady illumination: Real or illusory? *Perception, 32,* 1307–1310.

Pasternak, T., & Merigan, W. H. (1994). Motion perception following lesions of the superior temporal sulcus in the monkey. *Cerebral Cortex, 4,* 247–259.

Purves, D., Paydarfar, J. A., & Andrews, T. J. (1996). The wagon wheel illusion in movies and reality. *Proceedings of the National Academy of Sciences, U.S.A., 93,* 3693–3697.

Rees, G., Friston, K., & Koch, C. (2000). A direct quantitative relationship between the functional properties of human and macaque V5. *Nature Neuroscience, 3,* 716–723.

Reichardt, W. (1961). Autocorrelation, a principle for evaluation of sensory information by the central nervous system. In W. Rosenblith (Ed.), *Sensory communications*. New York: Wiley.

Roget, P. M. (1825). Explanation of an optical deception in the appearance of the spokes of a wheel seen through vertical apertures. *Philosophical Transactions of the Royal Society of London, 115,* 131–140.

Smith, A. T., Greenlee, M. W., Singh, K. D., Kraemer, F. M., & Hennig, J. (1998). The processing of first- and second-order motion in human visual cortex assessed by functional magnetic resonance imaging (fMRI). *Journal of Neuroscience, 18,* 3816–3830.

Smith, A. T., Wall, M. B., Williams, A. L., & Singh, K. D. (2006). Sensitivity to optic flow in human cortical areas MT and MST. *European Journal of Neuroscience, 23,* 561–569.

Stiers, P., De Cock, P., & Vandenbussche, E. (1998). Impaired visual perceptual performance on an object recognition task in children with cerebral visual impairment. *Neuropediatrics, 29,* 80–88.

Stiers, P., De Cock, P., & Vandenbussche, E. (1999). Separating visual perception and non-verbal intelligence in children with early brain injury. *Brain & Development, 21,* 397–406.

Stiers, P., van den Hout, B. M., Haers, M., Vanderkelen, R., de Vries, L. S., van Nieuwenhuizen, O., et al. (2001). The variety of visual perceptual impairments in pre-school children with perinatal brain damage. *Brain & Development, 23,* 333–348.

Talairach, J., & Tournoux, P. (1988). *Co-planar stereotaxic atlas of the human brain*. New York: Thieme.

Tassinari, G., Marzi, C. A., Lee, B. B., Di Lollo, V., & Campara, D. (1999). A possible selective impairment of magnocellular function in compression of the anterior visual pathways. *Experimental Brain Research, 127,* 391–401.

Tootell, R. B. H., Reppas, J. B., Kwong, K. K., Malach, R., Born, R. T., Brady, T. J., et al. (1995). Functional analysis of human MT and related visual cortical areas using magnetic resonance imaging. *Journal of Neuroscience, 15,* 3215–3230.

Vaina, L. M., Cowey, A., Jakab, M., & Kikinis, R. (2005). Deficits of motion integration and segregation in patients with unilateral extrastriate lesions. *Brain, 128,* 2134–2145.

Vaina, L. M., Cowey, A., & Kennedy, D. (1999). Perception of first- and second-order motion: Separable neurological mechanisms? *Human Brain Mapping, 7,* 67–77.

van den Hout, B. M., de Vries, L. S., Meiners, L. C., Stiers, P., van der Schouw, Y. T., Jennekens-Schinkel, A., et al. (2004). Visual perceptual impairment in children at 5 years of age with perinatal haemorrhagic or ischaemic brain damage in relation to cerebral magnetic resonance imaging. *Brain & Development, 26,* 251–261.

Van Oostende, S., Sunaert, S., Van Hecke, P., Marchal, G., & Orban, G. A. (1997). The kinetic occipital (KO) region in man: An fMRI study. *Cerebral Cortex, 7,* 690–701.

Volpe, J. (2001). *Neurology of the newborn*. United States: J.B. Saunders.

Watson, A. B., & Pelli, D. G. (1983). QUEST: A Bayesian adaptive psychometric method. *Perception & Psychophysics, 33,* 113–120.

Zeki, S., Watson, J. D., Lueck, C. J., Friston, K. J., Kennard, C., & Frackowiak, R. S. (1991). A direct demonstration of functional specialization in human visual cortex. *Journal of Neuroscience, 11,* 641–649.

Zeki, S. M. (1980). The response properties of cells in the middle temporal area (area MT) of owl monkey visual cortex. *Proceedings of the Royal Society of London, Series B, 207,* 239–248.